A Steep Slab at the Yap Trench Resulted from Subducting Oceanic Plateaus

Gaohua Zhu*[1,2], Hongfeng Yang[3,4], Xiang Gao[1,2], Dongdong Dong[1,2], Jianke Fan[1,2], Guangxu Zhang[1,2], and Cuilin Li[1,2]

Abstract

Interaction of oceanic plateaus with trenches plays a vital role in subduction activities and tectonic evolutions. The Yap trench is a rare case of an oceanic plateau subduction system. However, the knowledge of the impacts of plateau-trench interaction on subduction activity is still insufficient, due to a lack of seismological observations. Using ocean-bottom seismometer data near the Yap trench from April 2016 to May 2017, we conduct seismicity analyses in the Yap subduction zone by utilizing a machine-learning algorithm and matched-filter detections. The pattern of seismicity in the Yap trench exhibits characteristics similar to typical active subduction zones. The seismicity delineates a steep subducting slab, which may have resulted from the blocking of the buoyant Caroline Plateau. The majority of earthquakes are shallower than 80 km in the event-detectable area in the Yap trench, much shallower than the potential slab depth of 350 km from the previous seismic tomography images.

Cite this article as Zhu, G., H. Yang, X. Gao, D. Dong, J. Fan, G. Zhang, and C. Li (2024). A Steep Slab at the Yap Trench Resulted from Subducting Oceanic Plateaus, *Seismol. Res. Lett.* **96**, 473–483, doi: 10.1785/0220240051.

Supplemental Material

Introduction

The Yap trench–arc system is connected to the southern end of the Mariana subduction zone, which belongs to the continuous system of arcuate trenches in the western Pacific subduction zone (Fig. 1). The bathymetry of the Yap trench area has characteristics similar to other subduction zones in the western Pacific, such as island arc, back-arc basin, and deep trench (Fujiwara *et al.*, 2000). However, the Yap trench has distinct features, including a short trench–arc distance, limited intermediate depth seismicity, and absence of active arc volcanism (Hawkins and Batiza, 1977; Sato *et al.*, 1997; Fujiwara *et al.*, 2000; Ohara *et al.*, 2002; Zhang and Zhang, 2020). The trench–arc distance is only ~40 to 50 km, which is much shorter than in typical arc-trench systems with a mean distance of 166 ± 60 km (Fujiwara *et al.*, 2000; Stern, 2002). Seismicity along the Yap trench is very low compared to the Izu–Bonin–Mariana trenches, according to previous studies and unified global earthquake catalogs (Kobayashi, 2004; Xia *et al.*, 2020). In addition, there are no documented earthquakes deeper than 50 km along the Yap trench (Kobayashi, 2004; Zhang *et al.*, 2022).

With these distinct geophysical and geological characteristics, the activity of plate subduction at present along the Yap trench is in debate. As a rare case of oceanic plateau subduction system (Sato *et al.*, 1997), the Caroline Plateau is colliding with the Yap trench. The Caroline Plateau is further separated into the North and South Caroline Plateaus by the Sorol trough (Fig. 1). Dating the amphibolites along the Yap trench has suggested that the collision between the trench and Caroline Plateau occurred at ~21 Ma (Zhang and Zhang, 2020; Yao *et al.*, 2023). The Yap Islands are composed mainly of metamorphic rocks with minor volcanics, and arc volcanisms are considered to take place before 20–25 Ma with relative transient arc volcanism during 11–7 Ma (Fujiwara *et al.*, 2000; Ohara *et al.*, 2002; Kobayashi, 2004; Zhang and Zhang, 2020). Because of the lack of active-arc volcanism and deep-focus earthquakes, the subduction of the oceanic plate is thought to be halted by the collision of the Yap trench with the Caroline Plateau (Hawkins and Batiza, 1977; McCabe and Uyeda, 1983).

Conversely, some studies suggest that subduction along the Yap trench may still be active. For example, seismic observations revealed earthquakes distributed in the inner and outer trench slopes near the Yap trench, which is consistent with a typical pattern in active subduction zones (Sato *et al.*, 1997). In addition, heat flow values measured in the northern Yap region show a thermal profile largely compliant with that in normal subduction zones (Nagihara *et al.*, 1989; Kobayashi, 2004). The convergence rate is estimated to be small but ongoing, with a

1. Key Laboratory of Ocean Observation and Forecasting, Institute of Oceanology, Chinese Academy of Sciences, Qingdao, China, https://orcid.org/0000-0003-4186-7375 (GZ); https://orcid.org/0000-0002-0757-0650 (XG); https://orcid.org/0000-0002-8887-0187 (DD); https://orcid.org/0000-0002-8876-4659 (JF); https://orcid.org/0000-0003-0507-9910 (CL); 2. Laboratory for Marine Geology, Qingdao Marine Science and Technology Center, Qingdao, China; 3. Department of Earth and Environmental Science, Faculty of Science, The Chinese University of Hong Kong, Hong Kong, China, https://orcid.org/0000-0002-5925-6487 (HY); 4. Shenzhen Research Institute, The Chinese University of Hong Kong, Shenzhen, China

*Corresponding author: zhugaohua@qdio.ac.cn

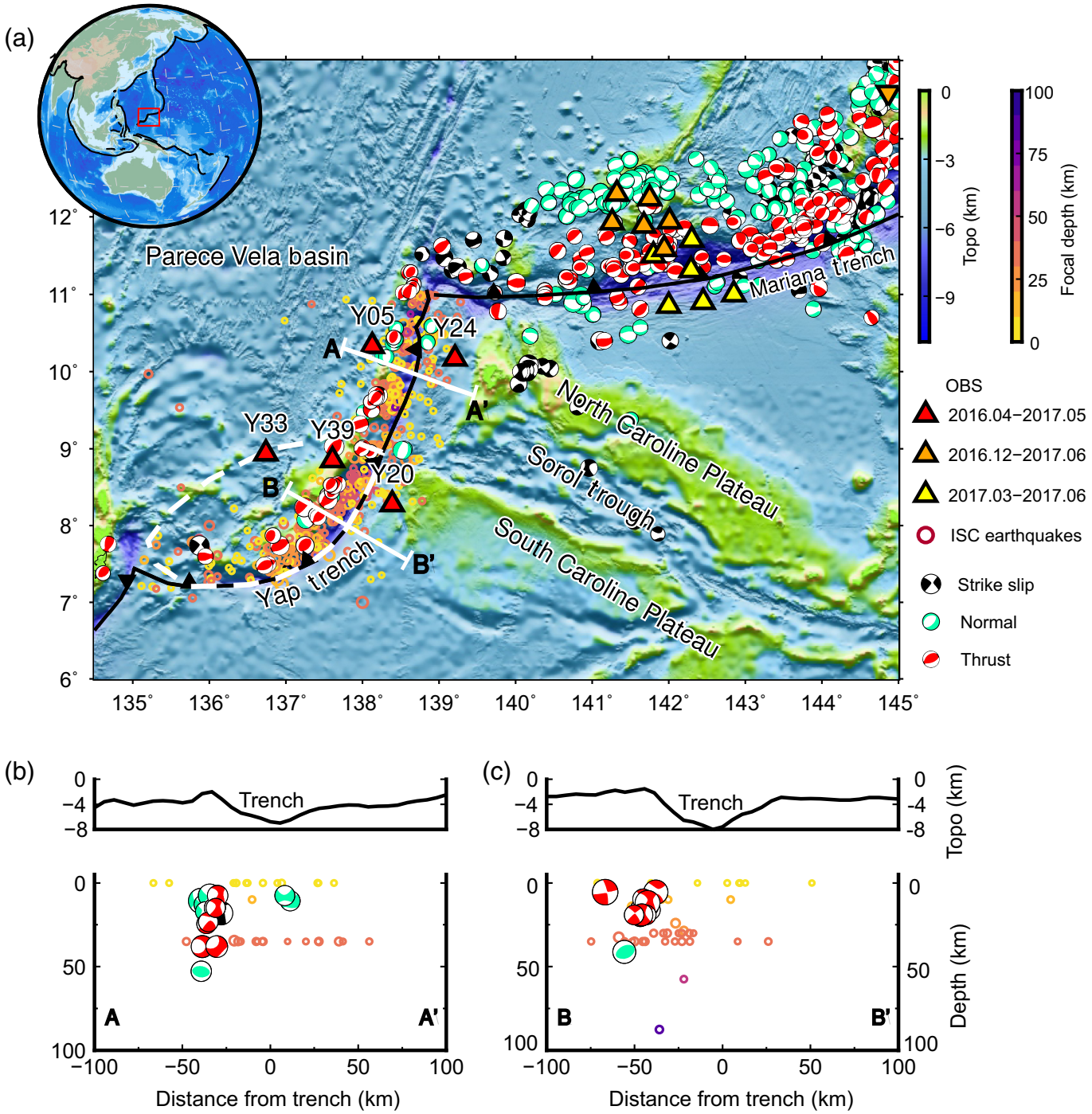

Figure 1. (a) Tectonic setting in and around the Yap trench and distribution of ocean-bottom seismometer (OBS, triangles) deployed and recovered around Yap and southern Mariana trench. The OBS around the Yap trench are shown in red triangles, which were operated from April 2016 to May 2017. Focal mechanism plots show moment tensor solutions from the Global Centroid Moment Tensor (Global CMT) catalog during 1978–2023, with thrust events in red, normal in Tiffany blue, and strike-slip events in black. The open dots represent earthquakes from the International Seismological Center (ISC) catalog colored by focal depth. The white dashed contour shows the inferred subducted South Caroline Plateau from Fan *et al.* (2022). The top inset map shows the location of the study area with the red frame marking the region. (b,c) Seismotectonics of the Yap trench area shown in cross-section views. The color version of this figure is available only in the electronic edition.

rate of less than 6 mm/yr along the Yap trench (Seno *et al.*, 1993). Besides, the lack of flat-lying layered sediments in the trench axis (Dong *et al.*, 2018), and the presence of metamorphic rocks in the Yap back-arc region also suggest active subduction (Lee, 2004; Chen *et al.*, 2019; Zhang and Zhang, 2020; Yao *et al.*, 2023). Therefore, these studies suggest that the Yap trench may be in early-stage subduction (Lee, 2004) or rejuvenated plate subduction (Zhang and Zhang, 2020).

Knowledge of the seismicity and geometry of subducting slabs is critical to the understanding of the Yap subduction activity and plateau-trench interaction. However, the resolution of historical earthquake locations from the International Seismological Center (ISC) along the Yap trench is limited (Fig. 1). Because of the paucity of seismic constraints, the spatial extent of the subducted slab is indistinct for the Yap trench, and there is also no information in the Slab2.0 model and several other global subduction zone geometry databases (Hayes *et al.*, 2018). Previous seismic studies located 67 events and did not record earthquakes with depth greater than 40 km during a 10-day ocean-bottom seismometer (OBS) observation (Sato *et al.*, 1997). In comparison, based on land and OBS observations, recent seismic tomographic results show that the subducting oceanic slab has overturned and extended down to a depth of ~350 km near the north of Yap Island (Fan *et al.*, 2022).

Although some investigations have been conducted near the Yap trench, comprehensive geophysical observations, especially seismological observations, are still scarce in the region. The distribution of seismicity and geometry of the subducting slab at the Yap trench remains largely unknown. In this article, we use the OBS data to obtain a local earthquake catalog from April 2016 to May 2017 in the Yap region. We first detect missing earthquakes using a machine-learning algorithm and matched-filter method, and then locate the detected earthquake. Our results provide valuable constraints on tectonic activity in the Yap trench and hold implications for the plateau-trench interaction.

Data and Methods

OBS data set and data corrections

A passive OBS array experiment was conducted in the Yap region from April 2016 to May 2017 (Fig. 1), using the research vessel Kexue from the Institute of Oceanology, Chinese Academy of Sciences (Zheng, Fan, Zhao, *et al.*, 2020; Fan *et al.*, 2022). Seven OBS sets were deployed, but only five of them with valid data were retrieved after the one-year-long observation. Each OBS set includes a three-component seismometer with a sampling rate of 50 Hz and a single-component hydrophone (Zheng, Fan, Zhao, *et al.*, 2020). Three of the OBSs were settled on the overriding plate, whereas the other two OBSs were deployed at the trench outer rise (Fig. 1).

The timing and horizontal orientation of OBSs have been corrected in previous studies (Zheng, Fan, Le, *et al.*, 2020; Zheng, Fan, Zhao, *et al.*, 2020). Timing correction is conducted based on ambient noise cross-correlation functions. The clock drifting of each OBS ranges from 1 to 3 s after one year deployment and changes linearly. The linear time correction is conducted for each OBS (Zheng, Fan, Le, *et al.*, 2020). Estimation of OBS orientation was conducted by fitting the amplitude of direct *P* wave of teleseismic receiver functions, and using the *P*-wave particle motion methods, as well as the Rayleigh-wave polarization method. The estimated results determined with various methods are generally consistent with each other (Zheng, Fan, Zhao, *et al.*, 2020). Timing-corrected OBS recordings can be illustrated by the well-aligned waveforms by their hypocentral distance for different teleseismic earthquakes in Figure 2 during the deployment.

Seismic phase detection and association

Because only four earthquakes were reported in the routine ISC earthquake catalog at the Yap trench area during the OBS deployment period, the template events were extremely incomplete for matched-filter detection. Therefore, to identify missing earthquakes, we first adopted the machine-learning algorithm–EQTransformer for earthquake phase detection (Mousavi *et al.*, 2020). Following the procedures in Zhu *et al.* (2023), we conducted a 1 Hz high-pass filter of the waveforms, which gives the best performance (i.e., with the highest recall and precision rate) on OBS data (Chen *et al.*, 2022). A threshold of 0.1 for *P* and *S* phases was typically adopted when using the EQTransformer. Considering lower signal-to-noise ratios (SNRs) of OBS data, we retained the predicted picks with a probability larger than 0.08 for the *P* and *S* phases, which can balance the aims of getting more phases and avoiding false detections. In total, 16,043 *P* and 18,019 *S* phases were predicted by EQTransformer.

The Rapid Earthquake Association and Location (REAL) algorithm was then used to associate the phase picks with individual events (Zhang *et al.*, 2019). Forty-two events with at least five phases (containing at least one *P* and one *S* phase) were associated and preliminarily located by the REAL algorithm (Fig. 3). Considering a large number of detected phases were not associated with events, the Gaussian Mixture Model Associator (GaMMA; Zhu *et al.*, 2022) was further used to associate the phase picks with individual events. The Gaussian mixture model improves phase association by considering multiple phase parameters, such as phase arrival time, phase amplitude, and phase picking quality score (Zhu *et al.*, 2022). The events with at least five phases (containing at least one *P* and one *S* phase) were preliminarily located, and events with less than five picks were discarded. In this process, 32 more events were associated with GaMMA (Fig. 3). A total of 74 events were identified and preliminarily located. The number of seismic phases required for associating events significantly influences the quantity of events. The number of associated events significantly increased, if required at

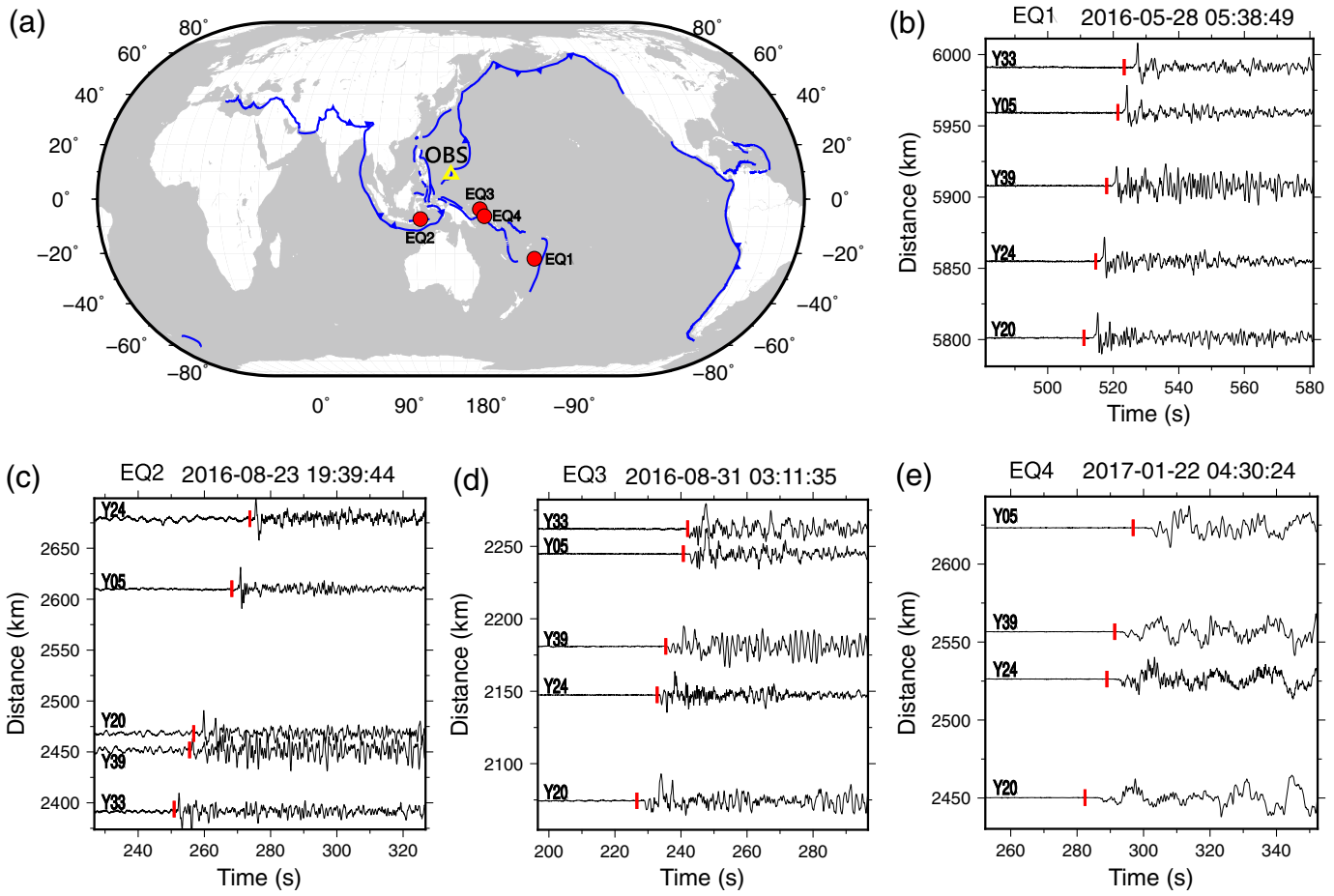

Figure 2. (a) The distribution of four example earthquakes for which waveforms are shown in panels (b–e). The yellow triangle represents the OBSs in the Yap trench. (b–e) Seismic waveforms of the four earthquakes in panel (a) recorded by vertical components of OBSs. The red bars mark the predicted *P*-wave arrivals. The station name is shown in the left of each waveform trace. The color version of this figure is available only in the electronic edition.

least four seismic phases (Fig. 3b). However, the events with only four seismic phases cannot be relocated in the following process; therefore, we adopted the GaMMA results with at least five phases.

Using the 74 earthquakes as template waveforms, we adopted matched-filter detection to further improve the detection, similar to previous studies (Peng and Zhao, 2009; Yang *et al.*, 2009; Zhu *et al.*, 2019). To improve the SNR of waveforms generated by local earthquakes, we applied a 2–8 Hz band-pass filter to both template waveforms and continuous OBS recordings. A 10 s time window (5 s before and 5 s after the *S* arrival) of previously identified earthquakes was selected as template waveforms. The threshold value of cross-correlation coefficient was 0.5 on a single station because this gives relatively stable detectability and can detect events with different spatial locations from template events. We combined detected events and removed duplicate detections with origin time within ±8 s. A total of 2138 earthquakes were detected after visual inspection.

Relocation of detected earthquakes

We then obtained absolute locations for earthquakes with clear first *P* and *S* arrivals on at least three stations using Hypoinverse (Klein, 2002) based on the IASP91 1D velocity model (Kennett and Engdahl, 1991). We have visually checked all the picked arrivals before relocation and assigned weight for picked arrivals. In addition, we also assigned distance weight and residual weight during location. The distance weighting function was 1.0 for stations closer than 200 km, followed a cosine taper, and then decreased to 0.0 for stations farther than 400 km. The residual weighting function was 1.0 for residuals <0.5 s, 0 for residuals >2 s, and also followed a cosine taper in between. We adopted the criterion that the horizontal and vertical errors were less than 20 and 50 km, respectively. A total of 712 out of the 2138 detected events were located using Hypoinverse. We compared the location difference between the ISC events and corresponding relocated events (Fig. S1, available in the supplemental material to this article). The time residuals were obviously reduced after relocation (Fig. S2), which demonstrates improved earthquake locations. Waveforms of an example event were also well aligned with

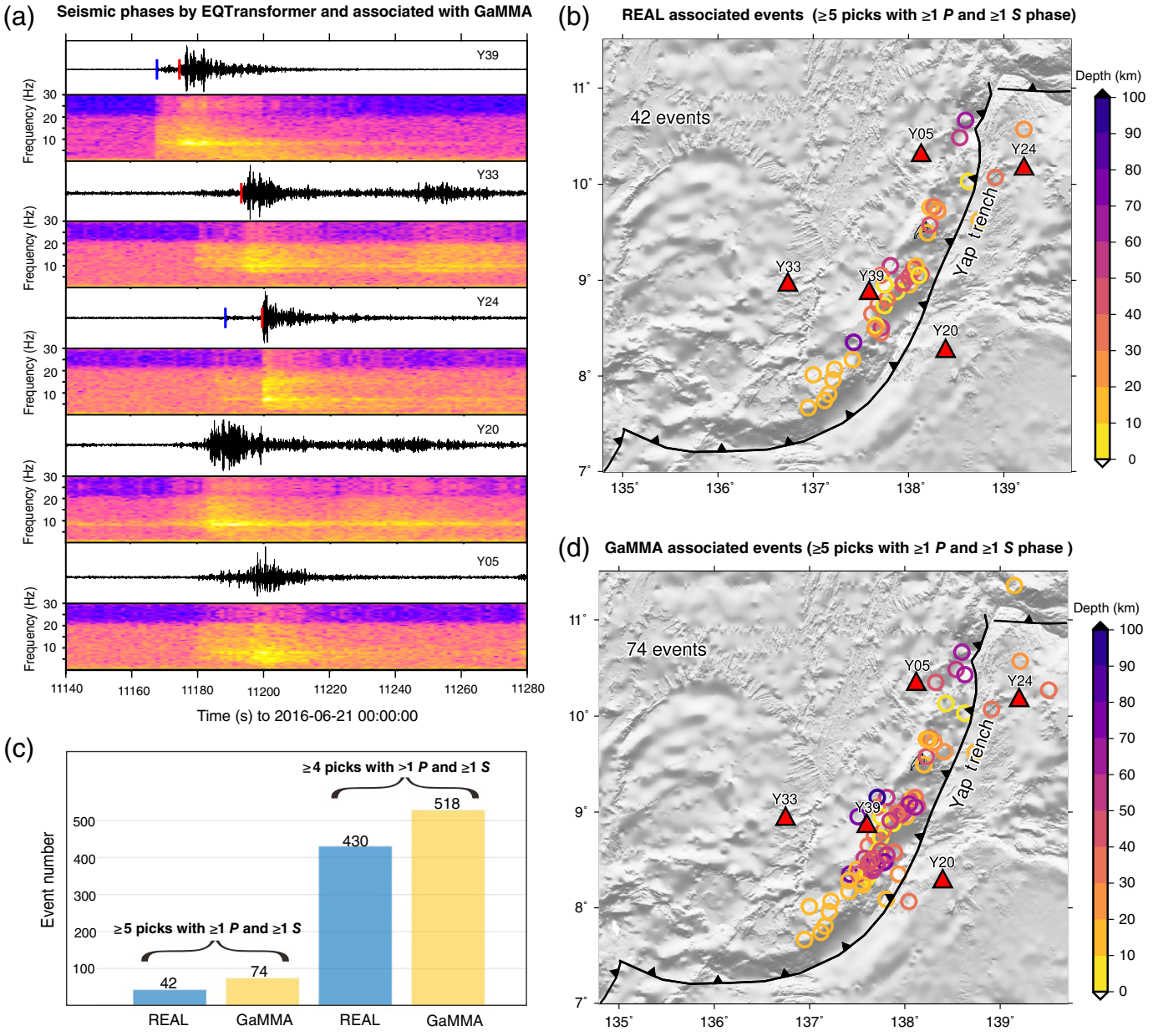

Figure 3. (a) Example event associated from the Gaussian Mixture Model Associator (GaMMA), with the predicted *P* and *S* phase marked by blue and red bars, respectively. (b,d) The distribution of earthquakes (circles) associated from the (b) Rapid Earthquake Association and Location (REAL) and (d) GaMMA. (c) Event association results from the REAL and GaMMA. The earthquakes were colored by focal depth. The color version of this figure is available only in the electronic edition.

hypocentral distance after relocation (Fig. S3). The average horizontal and vertical Hypoinverse location uncertainties are 4.0 and 12.9 km, respectively (Fig. S4).

We further improved the locations using the double-difference relocation–HypoDD algorithm (Waldhauser and Ellsworth, 2000), which can effectively reduce location errors due to structural variations and an imperfect velocity model. A total of 4143 *P*- and 2768 *S*-phase differential times were built from phase picks. We also measured differential travel times by cross correlating *P* and *S* waveforms of −1.5 to 2.5 s and −3 to 3 s, respectively, and got 70,584 *P*- and 34,691 *S*-wave differential time measurements. Both picked and cross-correlation-derived differential times were then used for the relocation, with a minimum number of eight for the differential time measurements per event pair and a maximum separation of 20 km. However, due to the small number of OBSs and large interstation distance, only 99 events near Y39 OBS were relocated using hypoDD eventually (Fig. S5). The average relative location uncertainties using hypoDD are 0.39, 0.44, and 0.56 km in the east–west, north–south, and vertical directions, respectively.

Because many detected events were only recorded by one or two nearest OBSs (Fig. S6), which cannot be located with

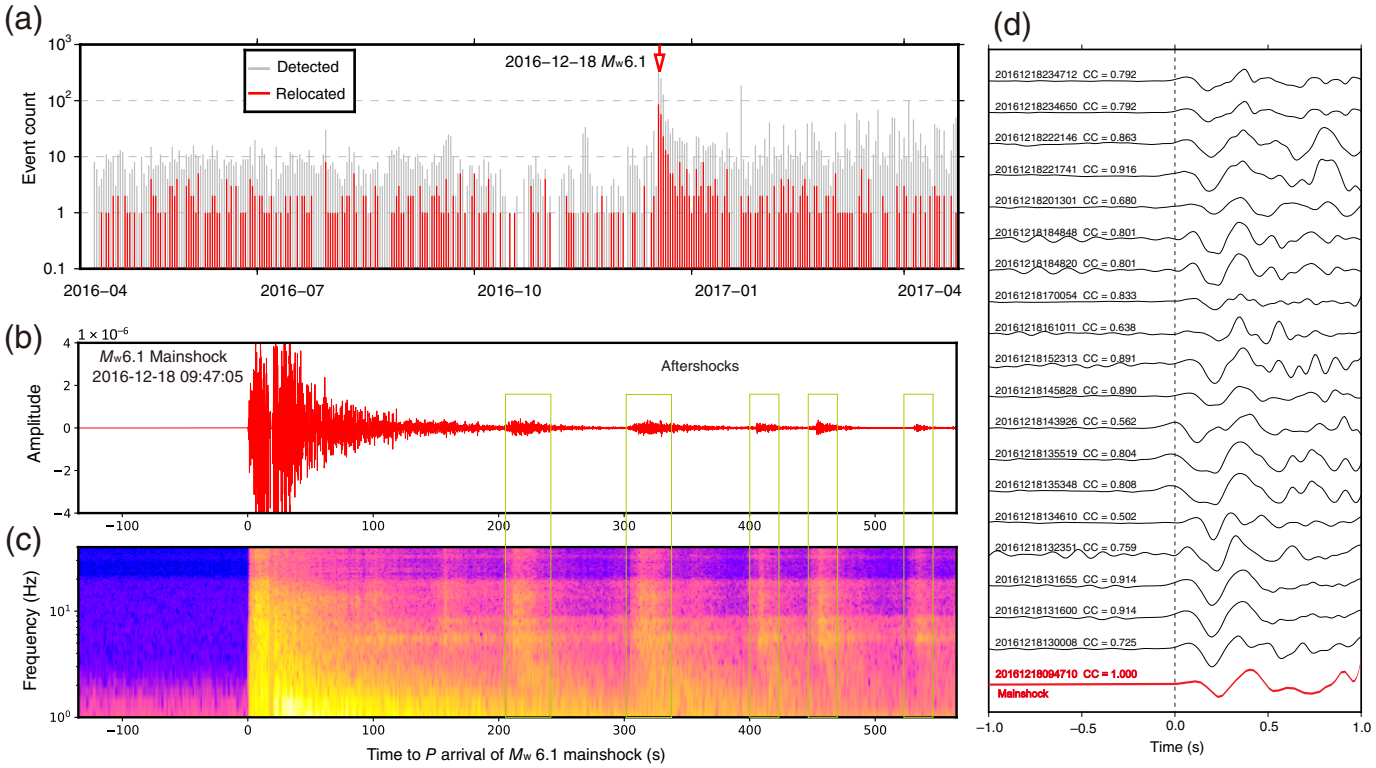

Figure 4. (a) The temporal distribution of located (red bars) and detected (gray bars) earthquakes. The vertical axis displays the number of events per day. The red arrow marks the day that the largest M_w 6.1 earthquake occurred. (b) Seismograms and (c) spectrograms of the M_w 6.1 mainshock and its aftershocks. (d) Seismograms of M_w 6.1 mainshock and some aftershocks recorded by Y39 OBS, which are aligned by *P* arrivals (0 s). The cross coefficient (CC) on top of each trace represents the cross coefficient of waveforms between the mainshock and aftershocks. The color version of this figure is available only in the electronic edition.

limited reliable phases, we combined 99 relocated events using hypoDD with the other events in their Hypoinverse locations. Therefore, 712 out of the 2138 detected events were located eventually during the one-year-long deployment in the Yap trench. There were a few to a dozen earthquakes every day (Fig. 4a). During the one-year-long observation, the largest M_w 6.1 earthquake occurred in December 2016, immediately following which a large number of aftershocks were observed (Fig. 4).

Resulting Seismicity Pattern

We can see some features of the spatial distribution of seismicity: a large number of earthquakes occurred in the inner trench slope, and some earthquakes occurred in the outer rise (Fig. 5). Beneath the Yap inner trench slope, the largest M_w 6.1 earthquake exhibits reverse slip according to the Global Centroid Moment Tensor (Global CMT) solution, with a centroid depth of 16 km (Fig. 5). Based on the distribution of Global CMT solutions, most of the earthquakes in the inner trench slope show thrust-faulting mechanisms (Fig. 1). Besides, in the trench outer-rise region, some earthquakes occurred within 30 km from the trench axis, with most focal depth shallower than 25 km.

We found many earthquakes with depths larger than 50 km, which can depict the potential location of the subducting plate. Based on the located seismicity, a steep subducting slab reaches ~80 km in depth, with nearly vertical dip angles (Fig. 6a–c). The slab-related earthquakes were horizontally concentrated within 60 km of the trench axis. The characteristics of seismicity along the Yap trench are quite different from the southern Mariana. Based on the earthquakes constrained by OBSs in southern Mariana during six months (Zhu *et al.*, 2019; Chen *et al.*, 2022), the slab-related earthquakes were horizontally distributed within ~150 km from the trench axis, and the deep subducted slab reaches ~240 km east of the Challenger Deep (Fig. 6f).

Discussion

Implications for oceanic plateau and trench interactions

The spatial distribution pattern of seismicity and slab geometry along the Yap trench was revealed, which can enhance our understanding of local tectonic activity and plateau subduction. About two hundredfold more earthquakes were detected than the global catalog in the Yap trench. A large number of earthquakes occurred beneath the inner trench

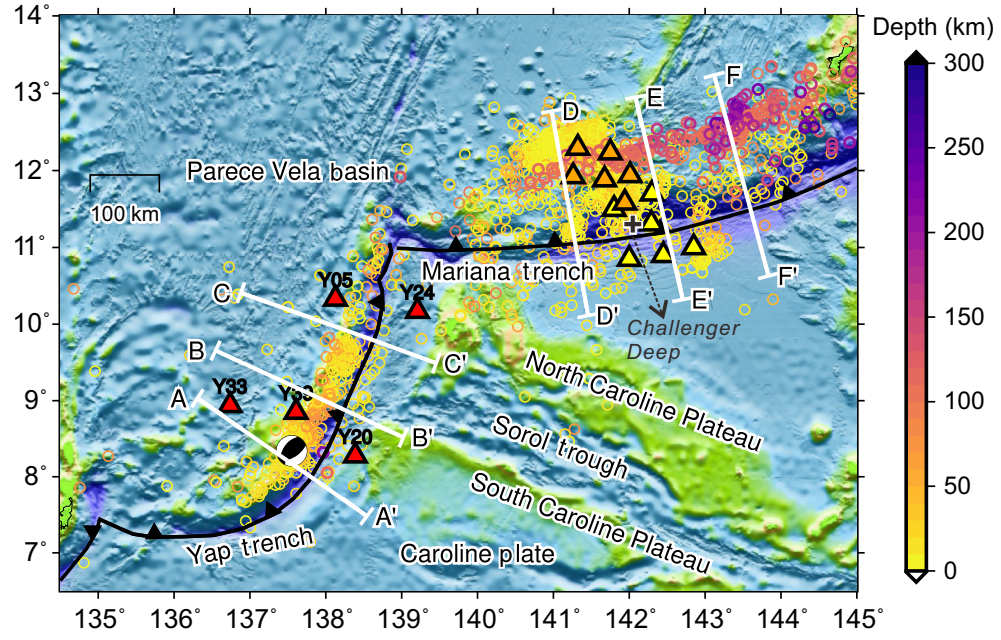

Figure 5. Map of relocated earthquakes (circles) colored by depth. The white cross symbol marks the Challenger Deep. The seismicity around the Mariana trench is from Zhu *et al.* (2019), which was also constrained by OBS data from December 2016 to June 2017 (orange triangles). The color version of this figure is available only in the electronic edition.

slope, and some of them show thrust-faulting mechanisms according to Global CMT solutions. Therefore, these earthquakes are most likely caused by thrusting relative motion between the overriding and subducting plate. Earthquakes occurred in the outer rise of the Yap trench, which is likely related to the bending faults (Zhang *et al.*, 2023). The occurrence of bending-related earthquakes and thrust-faulting earthquakes coincides with seismicity distribution in active subduction zones (Zhu *et al.*, 2019; Eimer *et al.*, 2020; Zhu *et al.*, 2023). These observations together with previous geochemical (Lee, 2004; Chen *et al.*, 2019; Zhang and Zhang, 2020; Yao *et al.*, 2023) and geophysical evidence (Nagihara *et al.*, 1989; Sato *et al.*, 1997; Kobayashi, 2004; Dong *et al.*, 2018) indicate ongoing plate subduction despite the Caroline Plateau collision.

The active subduction of the Caroline Plateau holds implications for the fate of an oceanic plateau, subducting into the mantle or accreting to the continental crust (Cloos, 1993; Yan *et al.*, 2022). The estimated crustal thickness for the South Caroline Plateau (near OBS Y20) is ~17.6 km using receiver functions, whereas the crustal thickness is ~8.5 km near OBS Y24 at the horst or garben structure zone (Fan *et al.*, 2022). Some previous studies expect that the arrival of an oceanic plateau (buoyant structure) into a subduction zone may block or even fail subduction (Arrial and Billen, 2013). In comparison, buoyancy analysis indicates that an oceanic plateau with a buoyant crustal thickness <15 km may subduct, but an oceanic plateau with a crustal thickness >30 km may not (Cloos, 1993). However, seismic and drill-core observations show that even the thickest Ontong Java plateau with a 30–40 km crust can subduct to depths of at least 200 km (Phinney *et al.*, 2004; Taylor and Benyshek, 2024). Although quantitative factors determining whether plateaus are accreted or subducted remain unclear, the potential of subducting an oceanic plateau may depend on the local isostatic balance of buoyancy forces, which is related to plate age and density, eclogitization of crustal basalt, and slab length (Cloos, 1993; Liu *et al.*, 2010, 2021; Arrial and Billen, 2013).

Subduction of buoyant Caroline Plateau has markedly affected the mode of subducted slab and interplate and intraplate earthquakes (Reyners *et al.*, 2011; Daly *et al.*, 2021; Yan *et al.*, 2021; Zhang *et al.*, 2021). Based on our observations of seismicity along the Yap trench, we suggested that the steep subducted slab is likely related to blocking of the buoyant Caroline Plateau near the Yap trench. The possible reason is that the buoyant oceanic plateau obstructs slab subduction near the trench, and the front of the subducted slab bends and sinks due to the relative larger density of the subducted slab compared with the asthenosphere (Yan *et al.*, 2022). Therefore, the subducted slab gradually steepens (Fig. 7). In addition, the high-angle subducted slab coincides well with the observations of steep arc-ward trench slope and intense bending-related faults in seismic profiles (Lee, 2004; Dong *et al.*, 2018), and the vertical slab images at depth < 100 km (Fan *et al.*, 2022).

The influences of subducting oceanic plateaus on slabs have also been reported by numerical models and observations. According to the numerical modeling, the behavior of a subducted slab may become steep or flat when an oceanic plateau interacts with a trench, mainly depending on the compositional density, mantle strength, and the size of an oceanic plateau (Arrial and Billen, 2013; Yan *et al.*, 2022). Seismic observations also indicate steepening of the subducted plate down-dip of the buoyant plateau (Reyners *et al.*, 2011; Taylor and Benyshek, 2024). The younger subducted Australian plate bends vertically, due to the collision of the Hikurangi Plateau with the northern Fiordland subduction zone near New Zealand (Reyners *et al.*, 2011). Besides, the subducted slabs constrained by seismicity are near vertical due to the

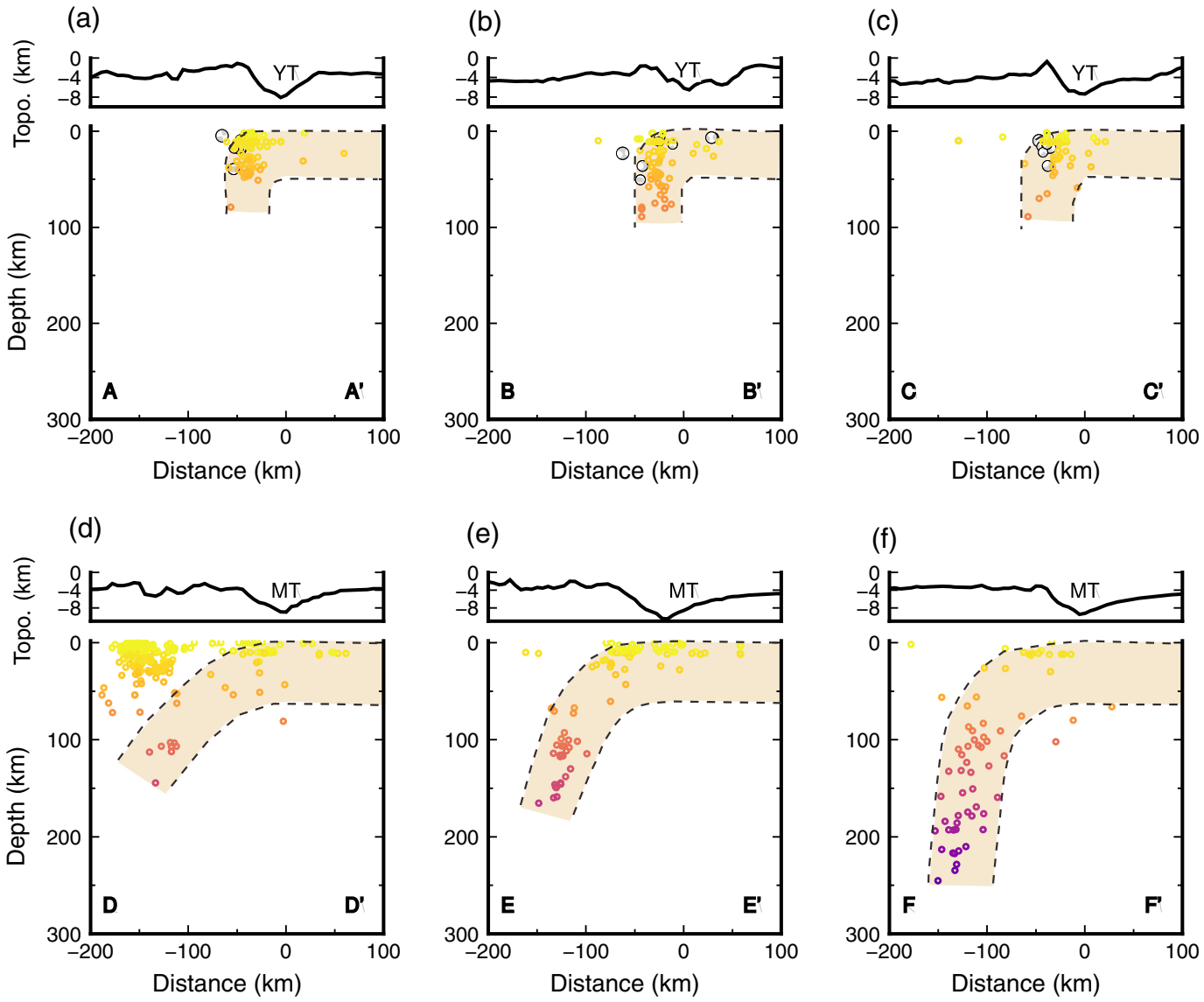

subduction of the Ontong Java Plateau under the Solomon Islands (Taylor and Benyshek, 2024).

In addition to the potential influences of an oceanic plateau on slab morphology, other possible mechanisms of steep subduction have been proposed by previous studies, such as the age and width of a subducted slab (Li *et al.*, 2011; Schellart, 2020). A compilation from the geological data of subduction zones in nature and results from the geodynamic subduction models both provide support for the hypothesis that subduction zone width and age play an important role in slab morphology, indicating that old (> ~80 to 100 Ma) and wide (≥ ~6000 km) subduction zones facilitate flat slab subduction, whereas narrow slabs retain steep dip angles (Schellart, 2020). The young Caroline plate (~35 to 30 Ma) and the narrow slab width (about 700 km; Fujiwara *et al.*, 2000) are favorable for steep slab subduction. Besides, other factors (e.g., overriding plate age and strength) related to wedge suction forces are also considered to influence slab subduction (Li *et al.*, 2011).

Figure 6. (a–f) Cross-section views with a bin width of 50 km of seismicity along the six profiles shown in Figure 5. Trench locations are marked as 0 km. Gray focal mechanism plots near the Yap trench show moment tensor solutions from the Global CMT. The light orange indicates a potential slab based on the located seismicity, but the dashed lines do not represent the boundary of the slab. MT, Mariana trench; YT, Yap trench. The color version of this figure is available only in the electronic edition.

Interpretations for limited earthquakes deeper than 80 km

The recorded seismicity in the Yap region shows most of the earthquakes shallower than 80 km. The deepest focal depths of earthquakes are shallower in the event-detectable area in the Yap trench, compared to southern Mariana with the deepest earthquake of ~240 km (Fig. 6). It is noted that limited observation period or detection power may be possible reasons

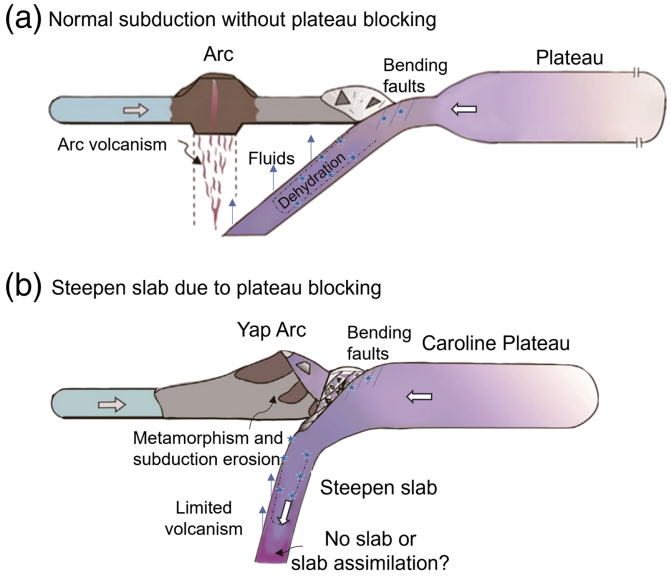

Figure 7. Schematic diagram of the steepening Yap subducted slab, modified after Zhang and Zhang (2020). (a) For normal subduction without plateau blocking, subducted slab dehydration promoted the generation of arc volcanism and initial arc. Blue stars represent earthquakes. (b) Because of the Caroline Plateau blocking slab subduction near the trench, the subducted slab steepens gradually as the front of subducted slab bends and sinks. With ultraslow subduction and a steep slab, the Yap arc-trench system is characterized by limited volcanism currently. The slow subducted slab may be assimilated into surrounding materials and become ductile, as shown in amaranth color. The color version of this figure is available only in the electronic edition.

for the absence of seismicity deeper than 80 km along the Yap trench, considering that the detectable deep earthquakes may be infrequent in a very slow convergent margin. However, the relative shallow earthquakes can also be revealed by global catalogs and a previous study (Sato *et al.*, 1997). Earthquake observations near the Yap trench using OBS for 10 days revealed some small earthquakes with hypocenters shallower than 40 km (Sato *et al.*, 1997). There is no earthquake deeper than 50 km, based on the hypocentral distribution from the Global CMT and ISC catalogs (Fig. 1). However, based on seismic tomography images, the slab is shallower than 100 km near the south Caroline Plateau, but is considered to reach a depth of 350 km near the north Caroline Plateau (Fan *et al.*, 2022). The observed seismicity is much shallower than the subducted slab imaged by seismic tomography near the north Caroline Plateau.

With our present understanding, lacking earthquakes deeper than 80 km is straightforward if there is no slab at depths larger than 80 km. Alternatively, if the subducted slab has reached deeper depths (e.g., 300 km) than observed earthquakes, other factors may lead to lacking earthquakes with depths > 80 km. Earthquakes deeper than 80 km occur at depths for which conventional frictional instability should not be possible; therefore, different mechanisms from shallow earthquakes may be responsible for the occurrence of intermediate-depth earthquakes (Zhan, 2020), such as dehydration embrittlement of metamorphosed oceanic crust and mantle (Peacock, 2001; Yamasaki and Seno, 2003; Frohlich, 2006) and thermal runaway (Wiens, 2001; Kelemen and Hirth, 2007). Besides, heterogeneous strain rate in slabs is proposed to be an influential factor in the depth distribution of seismicity, which can explain the large gaps in deep seismicity beneath ~300 to 550 km but do have earthquakes at depth from 500 to 660 km in Chile and Peru subduction zones (Billen, 2020). Therefore, we speculated that the hydration and dehydration state or thermal conditions may not favor failures of earthquakes deeper than 80 km at the Yap trench. Different from the convergence rate of 30–60 mm/yr in the Mariana trench (Stern *et al.*, 2004), the convergence rate along the Yap trench is very low (<6 mm/yr) due to the collision of Caroline Plateau (Seno *et al.*, 1993). The slow convergence rate allows sufficient slab assimilation, during which the characters of slab (such as temperature and mineral compositions) gradually approach to surrounding materials (Nagihara *et al.*, 1989). The slab may, therefore, become ductile due to increased temperature (Fig. 7). Moreover, the heated subducting slab may have completed dehydration of the main hydrous minerals such as antigorite at a shallow depth (Hacker *et al.*, 2003). These conditions are unfavorable for generating earthquakes at a deeper depth in the Yap trench.

Summary

Using a one-year-long OBS experiment near the Yap trench, we performed a machine-learning algorithm and matched-filter detections and constructed a comprehensive catalog of local earthquakes. Although only four earthquakes were reported in the ISC catalog during the deployment period, we found 2138 local earthquakes and located 712 out of them. A large number of earthquakes occurred in the inner trench slope, whereas some earthquakes occurred in the outer rise. These characteristics of seismicity in the Yap trench are generally similar to typical active subduction zones. Particularly, the seismicity delineates a nearly vertical subducted slab in the Yap trench, which is likely related to the blocking of the buoyant Caroline Plateau. Most focal depths are less than 80 km in the event-detectable area in the Yap trench, much shallower than the potential slab from seismic images in the same area. The reasons may stem from a limited observation period or detection power, lack of slab, or unfavorable thermal and petrological conditions for generating deep earthquakes.

Data and Resources

The earthquake catalog generated in this study is available online (https://figshare.com/articles/dataset/YapEarthquake/24920532). The seismograms of earthquakes can be accessed by connecting with the corresponding author. The historical earthquake catalog was collected from the International Seismological Center (ISC) Bulletin: event catalog search (http://www.isc.ac.uk/iscbulletin/search/catalogue/). The focal

mechanisms were from Global Centroid Moment Tensor (Global CMT) Project database (www.globalcmt.org/CMTsearch.html). All websites were last accessed in July 2024. The supplemental material for this article includes supporting figures of location uncertainties and comparison, and these figures are only available online.

Declaration of Competing Interests

The authors acknowledge that there are no conflicts of interest recorded.

Acknowledgments

The authors express our appreciation to the science parties and crew members of the Research vessel (R/V) KEXUE for the deployment and collection of the ocean-bottom seismometer (OBS) instruments. The authors also appreciate Guoliang Zhang, Zhonghai Li, Junhua Yao, and Ji Zhang for their helpful discussions. The authors are grateful to two anonymous reviewers for their constructive comments that improved the article. This study is supported by the National Natural Science Foundation of China (Grant Numbers 91958211, 92158205, 92258303, and 42106074), National Key R&D Program of China (Grant Number 2023YFF0806400), Shandong Province Outstanding Youth Science Fund Project Overseas (Grant Number 2023HWYQ-099), the Taishan Scholar Foundation of Shandong Province (tstp20230638), and Hong Kong Research Grants Council (Grant Number 14304820).

References

Arrial, P.-A., and M. I. Billen (2013). Influence of geometry and eclogitization on oceanic plateau subduction, *Earth Planet. Sci. Lett.* **363,** 34–43, doi: 10.1016/j.epsl.2012.12.011.

Billen, M. I. (2020). Deep slab seismicity limited by rate of deformation in the transition zone, *Sci. Adv.* **6,** no. 22, doi: 10.1126/sciadv.aaz7692.

Chen, H., H. Yang, G. Zhu, M. Xu, J. Lin, and Q. You (2022). Deep outer-rise faults in the southern Mariana subduction zone indicated by a machine-learning-based high-resolution earthquake catalog, *Geophys. Res. Lett.* **49,** no. 12, doi: 10.1029/2022gl097779.

Chen, L., L. Tang, X. Li, Y. Dong, X. Yu, and W. Ding (2019). Geochemistry of peridotites from the Yap Trench, Western Pacific: Implications for subduction zone mantle evolution, *Int. Geol. Rev.* **61,** no. 9, 1037–1051, doi: 10.1080/00206814.2018.1484305.

Cloos, M. (1993). Lithospheric buoyancy and collisional orogenesis: Subduction of oceanic plateaus, continental margins, island arcs, spreading ridges, and seamounts, *GSA Bull.* **105,** no. 6, 715–737.

Daly, K. A., G. A. Abers, M. E. Mann, S. Roecker, and D. H. Christensen (2021). Subduction of an oceanic plateau across southcentral Alaska: High-resolution seismicity, *J. Geophys. Res.* **126,** no. 11, doi: 10.1029/2021jb022809.

Dong, D., Z. Zhang, Y. Bai, J. Fan, and G. Zhang (2018). Topographic and sedimentary features in the Yap subduction zone and their implications for the Caroline Ridge subduction, *Tectonophysics* **722,** 410–421, doi: 10.1016/j.tecto.2017.11.030.

Eimer, M., D. A. Wiens, C. Cai, D. Lizarralde, and H. Jasperson (2020). Seismicity of the incoming plate and forearc near the Mariana Trench recorded by ocean bottom seismographs, *Geochem. Geophys. Geosys.* **21,** no. 4, doi: 10.1029/2020gc008953.

Fan, J., H. Zheng, D. Zhao, D. Dong, Y. Bai, C. Li, and Z. Zhang (2022). Seismic structure of the Caroline Plateau-Yap trench collision zone, *Geophys. Res. Lett.* **49,** no. 6, doi: 10.1029/2022gl098017.

Frohlich, C. (2006). *Deep Earthquakes*, Cambridge University Press, Cambridge, United Kingdom, doi: 10.1017/CBO9781107297562.

Fujiwara, T., C. Tamura, A. Nishizawa, K. Fujioka, K. Kobayashi, and Y. Iwabuchi (2000). Morphology and tectonics of the Yap Trench, *Mar. Geophys. Res.* **21,** nos. 1/2, 69–86, doi: 10.1023/a:1004781927661.

Hacker, B. R., S. M. Peacock, G. A. Abers, and S. D. Holloway (2003). Subduction factory 2. Are intermediate-depth earthquakes in subducting slabs linked to metamorphic dehydration reactions? *J. Geophys. Res.* **108,** no. B1, doi: 10.1029/2001jb001129.

Hawkins, J., and R. Batiza (1977). Metamorphic rocks of the Yap arc-trench system, *Earth Planet. Sci. Lett.* **37,** 216–229.

Hayes, G. P., G. L. Moore, D. E. Portner, M. Hearne, H. Flamme, M. Furtney, and G. M. Smoczyk (2018). Slab2, a comprehensive subduction zone geometry model, *Science* **362,** no. 6410, 58–61, doi: 10.1126/science.aat4723.

Kelemen, P. B., and G. Hirth (2007). A periodic shear-heating mechanism for intermediate-depth earthquakes in the mantle, *Nature* **446,** no. 7137, 787–790, doi: 10.1038/nature05717.

Kennett, B. L. N., and E. R. Engdahl (1991). Traveltimes for global earthquake location and phase identification, *Geophys. J. Int.* **105,** no. 2, 429–465, doi: 10.1111/j.1365-246X.1991.tb06724.x.

Klein, F. W. (2002). User's guide to HYPOINVERSE-2000, a Fortran program to solve for earthquake locations and magnitudes, *U.S. Geol. Surv. Open-File Rept. 02-171*, 123 pp.

Kobayashi, K. (2004). Origin of the Palau and Yap trench-arc systems, *Geophys. J. Int.* **157,** no. 3, 1303–1315, doi: 10.1111/j.1365-246X.2003.02244.x.

Lee, S.-M. (2004). Deformation from the convergence of oceanic lithosphere into Yap trench and its implications for early-stage subduction, *J. Geodynam.* **37,** no. 1, 83–102, doi: 10.1016/j.jog.2003.10.003.

Li, Z. H., Z. Q. Xu, and T. V. Gerya (2011). Flat versus steep subduction: Contrasting modes for the formation and exhumation of high- to ultrahigh-pressure rocks in continental collision zones, *Earth Planet. Sci. Lett.* **301,** nos. 1/2, 65–77, doi: 10.1016/j.epsl.2010.10.014.

Liu, L., M. Gurnis, M. Seton, J. Saleeby, R. D. Müller, and J. M. Jackson (2010). The role of oceanic plateau subduction in the Laramide orogeny, *Nature Geosci.* **3,** no. 5, 353–357, doi: 10.1038/ngeo829.

Liu, Z., L. Dai, S. Li, L. Wang, H. Xing, Y. Liu, F. Ma, H. Dong, and F. Li (2021). When plateau meets subduction zone: A review of numerical models, *Earth Sci. Rev.* **215,** 103556, doi: 10.1016/j.earscirev.2021.103556.

McCabe, R., and S. Uyeda (1983). Hypothetical model for the bending of the Mariana Arc, in *The Tectonic and Geologic Evolution of Southeast Asian Seas and Islands: Part 2*, D. E. Hayes (Editor), Vol. 27, Geophysical Monograph Series, doi: 10.1029/GM027p0281.

Mousavi, S. M., W. L. Ellsworth, W. Zhu, L. Y. Chuang, and G. C. Beroza (2020). Earthquake transformer-an attentive deep-learning model for simultaneous earthquake detection and phase picking, *Nat. Commun.* **11,** no. 1, 3952, doi: 10.1038/s41467-020-17591-w.

Nagihara, S., M. Kinoshita, H. Fujimoto, H. Katao, H. Kinoshita, and Y. Tomoda (1989). Geophysical observations around the northern Yap Trench: Seismicity, gravity and heat flow, *Tectonophysics* **163,** nos. 1/2, 93–104, doi: 10.1016/0040-1951(89)90120-0.

Ohara, Y., K. Fujioka, O. Ishizuka, and T. Ishii (2002). Peridotites and volcanics from the Yap arc system: Implications for tectonics of the southern Philippine Sea Plate, *Chem. Geol.* **189,** nos. 1/2, 35–53, doi: 10.1016/s0009-2541(02)00062-1.

Peacock, S. M. (2001). Are the lower planes of double seismic zones caused by serpentine dehydration in subducting oceanic mantle? *Geology* **29,** no. 4, 299–302.

Peng, Z., and P. Zhao (2009). Migration of early aftershocks following the 2004 Parkfield earthquake, *Nature Geosci.* **2,** no. 12, 877–881, doi: 10.1038/ngeo697.

Phinney, E. J., P. Mann, M. F. Coffin, and T. H. Shipley (2004). Sequence stratigraphy, structural style, and age of deformation of the Malaita accretionary prism (Solomon arc–Ontong Java Plateau convergent zone), *Tectonophysics* **389,** no. 3, 221–246, doi: 10.1016/j.tecto.2003.10.025.

Reyners, M., D. Eberhart-Phillips, and S. Bannister (2011). Tracking repeated subduction of the Hikurangi Plateau beneath New Zealand, *Earth Planet. Sci. Lett.* **311,** nos. 1/2, 165–171, doi: 10.1016/j.epsl.2011.09.011.

Sato, T., J. Kasahara, H. Katao, N. Tomiyama, K. Mochizuki, and S. Koresawa (1997). Seismic observations at the Yap Islands and the northern Yap Trench, *Tectonophysics* **271,** nos. 3/4, 285–294, doi: 10.1016/s0040-1951(96)00251-x.

Schellart, W. P. (2020). Control of subduction zone age and size on flat slab subduction, *Front. Earth Sci.* **8,** 26, doi: 10.3389/feart.2020.00026.

Seno, T., S. Stein, and A. E. Gripp (1993). A model for the motion of the Philippine Sea Plate consistent with NUVEL-1 and geological data, *J. Geophys. Res.* **98,** no. B10, 17,941–17,948, doi: 10.1029/93jb00782.

Stern, R. J. (2002). Subduction zones, *Rev. Geophys.* **40,** no. 4, 1012, doi: 10.1029/2001RG000108.

Stern, R. J., M. J. Fouch, and S. L. Klemperer (2004). An overview of the Izu-Bonin-Mariana subduction factory, in *Inside the Subduction Factory*, J. Eiler (Editor), doi: 10.1029/138GM10.

Taylor, B., and E. K. Benyshek (2024). Oceanic plateau and spreading ridge subduction accompanying arc reversal in the Solomon Islands, *Geochem. Geophys. Geosys.* **25,** no. 1, doi: 10.1029/2023gc011270.

Waldhauser, F., and W. L. Ellsworth (2000). A double-difference earthquake location algorithm: Method and application to the Northern Hayward Fault, California, *Bull. Seismol. Soc. Am.* **90,** no. 6, 1353–1368, doi: 10.1785/0120000006.

Wiens, D. A. (2001). Seismological constraints on the mechanism of deep earthquakes: temperature dependence of deep earthquake source properties, *Phys. Earth Planet. In.* **127,** nos. 1/4, doi: 10.1016/s0031-9201(01)00225-4.

Xia, C. L., Y. P. Zheng, B. H. Liu, Q. F. Hua, K. Liu, L. Ma, and X. F. Li (2020). Geological and geophysical differences between the north and south sections of the Yap trench-arc system and their relationship with Caroline Ridge subduction, *Geol. J.* **55,** no. 12, 7775–7789, doi: 10.1002/gj.3903.

Yamasaki, T., and T. Seno (2003). Double seismic zone and dehydration embrittlement of the subducting slab, *J. Geophys. Res.* **108,** no. B4, doi: 10.1029/2002jb001918.

Yan, Z., L. Chen, X. Xiong, B. Wan, and H. Xu (2021). Oceanic plateau and subduction zone jump: Two-dimensional thermo-mechanical modeling, *J. Geophys. Res.* **126,** no. 7, doi: 10.1029/2021jb021855.

Yan, Z., L. Chen, A. V. Zuza, J. Tang, B. Wan, and Q. Meng (2022). The fate of oceanic plateaus: Subduction versus accretion, *Geophys. J. Int.* **231,** no. 2, 1349–1362, doi: 10.1093/gji/ggac266.

Yang, H., L. Zhu, and R. Chu (2009). Fault-plane determination of the 18 April 2008 Mount Carmel, Illinois, earthquake by detecting and relocating aftershocks, *Bull. Seismol. Soc. Am.* **99,** no. 6, 3413–3420, doi: 10.1785/0120090038.

Yao, J., G. Zhang, J. Zhang, and D.-F. He (2023). Petrological and geochemical constraints of mantle peridotites on the magma-starved Yap Arc formed by ultra-slow subduction, *Contrib. Mineral. Petrol.* **178,** no. 11, doi: 10.1007/s00410-023-02056-2.

Zhan, Z. (2020). Mechanisms and implications of deep earthquakes, *Annu. Rev. Earth Planet. Sci.* **48,** no. 1, 147–174, doi: 10.1146/annurev-earth-053018-060314.

Zhang, J., and G. Zhang (2020). Geochemical and chronological evidence for collision of proto-Yap arc/Caroline plateau and rejuvenated plate subduction at Yap trench, *Lithos* **370,** 105616, doi: 10.1016/j.lithos.2020.105616.

Zhang, J., H. Yang, G. Zhu, H. Chen, F. Zhang, and Z. Sun (2023). The effect of along-strike variable plate deflection on bending stress and seismicity at the southern Mariana Trench, *Tectonophysics* doi: 10.1016/j.tecto.2023.229752.

Zhang, J., F. Zhang, H. Yang, J. Lin, and Z. Sun (2021). The effects of plateau subduction on plate bending, stress and intraplate seismicity, *Terra Nova* **34,** no. 2, 113–122, doi: 10.1111/ter.12570.

Zhang, M., W. L. Ellsworth, and G. C. Beroza (2019). Rapid earthquake association and location, *Seismol. Res. Lett.* **90,** no. 6, 2276–2284, doi: 10.1785/0220190052.

Zhang, Z., S. Li, G. Wang, Y. Suo, G. Wang, and P. Wang (2022). Plate boundary processes of the Caroline Plate, *Sci. China Earth Sci.* **65,** no. 8, 1554–1567, doi: 10.1007/s11430-021-9919-6.

Zheng, H., J. Fan, B. M. Le, T. Yang, C. Li, X. Wang, and D. Dong (2020). Time correction of Ocean Bottom Seismometer (OBS) deployed at the Yap subduction zone using ambient noise cross-correlation, *Prog. Geophys.* **35,** no. 2, 799–806.

Zheng, H., J. Fan, D. Zhao, C. Li, D. Dong, G. Zhang, and X. Wang (2020). A new method to estimate ocean-bottom-seismometer orientation using teleseismic receiver functions, *Geophys. J. Int.* **221,** no. 2, 893–904, doi: 10.1093/gji/ggaa041.

Zhu, G., H. Yang, J. Lin, Z. Zhou, M. Xu, J. Sun, and K. Wan (2019). Along-strike variation in slab geometry at the southern Mariana subduction zone revealed by seismicity through ocean bottom seismic experiments, *Geophys. J. Int.* **218,** no. 3, 2122–2135, doi: 10.1093/gji/ggz272.

Zhu, G., H. Yang, T. Yang, and G. Zhang (2023). Along-strike variation of seismicity near the extinct mid-ocean ridge subducted beneath the Manila Trench, *Seismol. Res. Lett.* **94,** no. 2A, 792–804, doi: 10.1785/0220220304.

Zhu, W., I. W. McBrearty, S. M. Mousavi, W. L. Ellsworth, and G. C. Beroza (2022). Earthquake phase association using a Bayesian Gaussian Mixture Model, *J. Geophys. Res.* **127,** no. 5, e2021JB023249, doi: 10.1029/2021JB023249.

Manuscript received 6 February 2024
Published online 21 August 2024